Geophys. J. Int. (1999) **139,** 216–226

Implications of a ductile crustal layer for the deformation caused by the Fennoscandian ice sheet

Volker Klemann[1] and Detlef Wolf[2]

[1] *University of Münster, Institute of Planetology, Wilhelm-Klemm-Strasse* 10, D-48149 *Münster, Germany. E-mail: volkerk@uni-muenster.de*
[2] *GeoForschungsZentrum Potsdam, Kinematics and Dynamics of the Earth, Telegrafenberg,* D-14473 *Potsdam, Germany*

Accepted 1999 May 27. Received 1999 April 6; in original form 1998 June 12

SUMMARY

Previous studies of glacial–isostatic adjustment have usually considered earth models with a purely elastic lithosphere. A possibly significant deviation from this assumption is the presence of a ductile crustal layer embedded in an otherwise elastic lithosphere. Such a layer has been suggested for various continental regions on the basis of seismic and tectonic evidence. The present study investigates the implications of a ductile crustal layer for the interpretation of glacial–isostatic adjustment using a layered, incompressible Maxwell viscoelastic earth model and a simplified representation of the Fennoscandian glaciation. The relaxation-time and amplitude spectra show that, besides the conventional buoyancy mode M0 also present in earth models with a purely elastic lithosphere, the ductile layer supports a slowly decaying mode MC, which is capable of modifying the deformation markedly. Thus, measures of the *absolute* deformation such as the stress clearly reflect the presence of the ductile layer. In contrast to this are measures of the *relative* deformation such as the vertical displacement rate and the rate of gravity change. To a good approximation, these rates are inversely proportional to the relaxation time of the more quickly decaying mode M0, and are, therefore, less affected by the ductile layer. Taken together, the present study suggests that, provided a ductile crustal layer exists, its presence should be accounted for in interpretations of the glacial–isostatic adjustment following the Fennoscandian or smaller glaciations.

Key words: crustal deformation, glacial rebound, lithospheric flexure, viscoelasticity.

1 INTRODUCTION

According to mineralogical and thermodynamic considerations, solid-state creep in crustal materials is expected to become active at relatively low temperatures of ~ 350 °C (e.g. De Rito *et al.* 1986). The constitutive equation describing these creep processes has been inferred from laboratory experiments, which suggest a *power-law* relation between the maximum shear stress and the strain rate (e.g. Weertman 1978). However, due to technical restrictions, all experiments have been performed at rather high shear stresses in the range 10–100 MPa, resulting in relatively high strain rates of $\sim 10^{-8}$ s^{-1}. The extrapolation of the laboratory results to the much smaller strain rates of $\sim 10^{-15}$ s^{-1} typical of geodynamic processes is uncertain and, therefore, a *linear* relation between the maximum shear stress and the strain rate cannot be excluded (e.g. Ranalli & Murphy 1987; Kohlstedt *et al.* 1995).

Independent of these studies, the problem of the existence of a ductile crustal layer has also been addressed using geophysical results. Circumstantial evidence of the presence of such a layer is the lack of seismicity in the lower crust found in various tectonic provinces (e.g. Vetter & Meissner 1979; Meissner & Strehlau 1982; Chen & Molnar 1983) and possibly also in Fennoscandia (e.g. Slunga 1989; Arvidsson 1996) or an increase of seismic reflectors in the lower crust, indicating lamination supported by ductile flow (Meissner & Wever 1986). Although a noticeable influence of a ductile crustal layer on geodynamic processes can be expected, investigations of its significance have so far been largely limited to long-period processes (characteristic times of $\sim 10^6$–10^8 yr) such as rifting and plate collision (e.g. Kruse *et al.* 1991; Lobkovsky & Kerchman 1991) or the evolution of sedimentary basins (e.g. Kaufman & Royden 1994). For short-period processes (characteristic times of $\sim 10^2$ yr), the stress relaxation of post-seismic events (Rydelek & Sacks 1990; Rydelek & Pollitz 1994) or the isostatic adjustment in response to mining activity (Klein *et al.* 1997) have been used to infer the rheology of the lower crust. In contrast to these examples are glacial–isostatic adjustment processes in response to the Pleistocene glaciations (characteristic times of $\sim 10^4$–10^6 yr), where investigations

into the implications of a ductile crustal layer are largely lacking. An exception is the study by Wu (1997), who investigated the influence of a ductile layer within the lithosphere on the stress field in eastern Canada.

The objective of the present paper is to quantify the implications of a ductile crustal layer for the interpretation of observations of glacial–isostatic adjustment. Similar to Wu (1997), we restrict our study to linear creep processes and use the theory developed for an incompressible *Maxwell viscoelastic* half-space subjected to surface loading; in contrast to him, we base our results on an analytical solution and assume a smaller viscosity in the ductile crustal layer than in the upper mantle (Section 2). Upon comparing the responses of earth models with or without a ductile layer in the spectral domain (Section 3), we consider as an important example the Pleistocene Fennoscandian glaciations and predict the various signatures of the readjustment process following the last deglaciation for the two earth models in the spatial domain (Section 4). Our study concludes with a brief summary of the main results obtained (Section 5).

2 THEORETICAL MODEL

The field theory used in this study describes the quasi-static response of a homogeneously layered, incompressible Maxwell viscoelastic half-space subjected to surface loading. Upon Laplace transformation with respect to time, t, we obtain a second-order differential system (eq. A1). Using cylindrical coordinates, (r, φ, z), where r is the radial distance from the load axis, φ the azimuth and z the depth, and assuming axisymmetric loading, the dependence on φ vanishes. Finally, taking the Hankel transform with respect to r, the mathematical formulation of the problem can be recast into a first-order differential matrix system that, for each homogeneous layer, takes the form

$$\frac{d}{dz}\,\tilde{\mathbf{Y}}(k, z, s) = \mathbf{A}(k, s)\tilde{\mathbf{Y}}(k, z, s)\,. \tag{1}$$

In this equation, $\tilde{\mathbf{Y}}(k, z, s)$ is the *Laplace-* and *Hankel-transformed* solution vector containing the transformed displacement and stress components, $\mathbf{A}(k, s)$ is a 4×4 matrix whose components characterize the viscoelastic properties of the particular layer, k is the Hankel wavenumber and s is the inverse Laplace time. Upon application of appropriate boundary, interface and regularity conditions, the solution to eq. (1) can be expressed in analytic form.

Assuming a Heaviside loading event, $H(t)$, and taking the inverse Laplace transform, physical insight can be gained from a discussion of the solution functions in the *spectral* (k, z, t) domain. Considering, in particular, the zeroth-order Hankel transform of the (downward) vertical displacement, $W^{[0]}(k, z, t)$, the first-order Hankel transform of the (outward) horizontal displacement, $U^{[1]}(k, z, t)$, and the zeroth-order Hankel transform of the load pressure, $Q^{[0]}(k)H(t)$, we define *normalized* displacements according to

$$W(k, z, t) := \rho_{\mathrm{UM}}\, g\, \frac{W^{[0]}(k, z, t)}{Q^{[0]}(k)}\,, \tag{2}$$

$$U(k, z, t) := \rho_{\mathrm{UM}}\, g\, \frac{U^{[1]}(k, z, t)}{Q^{[0]}(k)}\,, \tag{3}$$

with g the gravity and ρ_{UM} the upper mantle density. Note that, since $W^{[0]}/Q^{[0]} = 1/(\rho_{\mathrm{UM}}g)$ applies to a fluid half-space with density ρ_{UM}, the displacements have been normalized such that $W(k, 0, t) = 1$ applies to this case. For the homogeneously layered, incompressible Maxwell viscoelastic half-space considered, the explicit expressions for $W(k, z, t)$ and $U(k, z, t)$ take the forms

$$W(k, z, t) = W^{\mathrm{E}}(k, z) + \sum_{m=1}^{M} W_m^{\mathrm{V}}(k, z)\,[1 - \mathrm{e}^{-t/\tau_m(k)}]\,, \tag{4}$$

$$U(k, z, t) = U^{\mathrm{E}}(k, z) + \sum_{m=1}^{M} U_m^{\mathrm{V}}(k, z)\,[1 - \mathrm{e}^{-t/\tau_m(k)}]\,, \tag{5}$$

where $W^{\mathrm{E}}(k, z)$ and $U^{\mathrm{E}}(k, z)$ are the *elastic* amplitudes for displacement, $W_m^{\mathrm{V}}(k, z)$ and $U_m^{\mathrm{V}}(k, z)$ are the *viscous* amplitudes for displacement, $\tau_m(k)$ is the relaxation time and $t > 0$ is assumed. The corresponding *fluid* amplitudes are defined by

$$W^{\mathrm{F}}(k, z) := W^{\mathrm{E}}(k, z) + \sum_{m=1}^{M} W_m^{\mathrm{V}}(k, z)\,, \tag{6}$$

$$U^{\mathrm{F}}(k, z) := U^{\mathrm{E}}(k, z) + \sum_{m=1}^{M} U_m^{\mathrm{V}}(k, z)\,. \tag{7}$$

Comparing eqs (4) and (5) with eqs (6) and (7), respectively, we notice that $W^{\mathrm{E}}(k, z)$ and $U^{\mathrm{E}}(k, z)$ are the initial displacements for $t \to 0$ and $W^{\mathrm{F}}(k, z)$ and $U^{\mathrm{F}}(k, z)$ the final displacements for $t \to \infty$. The transition from the elastic response to the fluid response is described by a series of exponential functions. Their total number, M, and the individual amplitudes and relaxation times define the set of eigenfunctions and eigenvalues of the differential system and are related to the particular layering considered (Tromp & Mitrovica 1999a; Appendix A).

The calculation of the response in the *spatial* (r, z, t) domain for arbitrary loads requires multiplication with the Hankel-transformed load pressure, inverse Hankel transformation and convolution in time with the loading history (for details see Wolf 1985 and Breuer & Wolf 1995).

In this study, we use the four-layer earth model VC, consisting of an elastic upper crust, a viscoelastic lower crust simulating a ductile crustal layer, an elastic mantle lithosphere and a viscoelastic substratum simulating the upper mantle (Table 1). The viscosity of the lower crust, $\eta_{\mathrm{LC}} = 10^{17}$ Pa s, and its thickness, $h_{\mathrm{LC}} = 10$ km, are based on estimates by Meissner & Strehlau (1982), Kaufman & Royden (1994) and others. The values chosen for the density, ρ, and the shear modulus, μ, of the individual layers and for the viscosity of the upper mantle,

Table 1. Parameter values of the earth models used.

	ρ (kg m^{-3})	μ (GPa)	η (Pa s)	h (km)
Earth model VC				
Upper crust	2900	64.0	∞	35
Lower crust	2900	64.0	1.0×10^{17}	10
Mantle lithosphere	3380	64.0	∞	65
Upper mantle	3380	145.0	1.0×10^{21}	∞
Earth model EC				
Crust	2900	64.0	∞	45
Mantle lithosphere	3380	64.0	∞	65
Upper mantle	3380	145.0	1.0×10^{21}	∞

η_{UM}, are similar to standard values used in the literature. For comparison, we also consider the three-layer earth model EC, in which the ductile crustal layer is absent and, therefore, the lithosphere is purely elastic (Table 1).

3 COMPUTATIONAL RESULTS: SPECTRAL DOMAIN

We begin with a discussion of the solution vector in the spectral domain and consider in particular the vertical and horizontal surface displacements for a Heaviside loading event. Fig. 1 shows spectra of the relaxation times, the elastic amplitudes, the viscous amplitudes and the fluid amplitudes for earth models VC and EC. For convenient comparison with the solutions available for spherical earth models, the *normalized* Hankel wavenumber, $n := ka$, where a is the earth radius, is used. Besides the exponential contributions to the displacement calculated according to eqs (4) and (5), the (physical) viscous *modes* associated with the characteristic features of the viscoelastic stratification are distinguished. Before we discuss the viscous modes more closely, it is necessary to explain their classification. This is based on the *Lagrangian* of the momentum equation (e.g. Backus & Gilbert 1967; Peltier 1976; Tromp & Mitrovica 1999b), which leads to expressions of the shear-potential density, $M(z)$, and the gravitational-potential density, $R(z)$ (Appendix A). In the following, we discriminate between *buoyancy* modes, which show significant magnitude in $M(z)$ and $R(z)$, and *viscoelastic* modes, which show significant magnitude only in $M(z)$.

Fig. 2 shows the potential densities of the viscous modes for earth models VC and EC and for the wavenumbers $n = 2$, 20 and 200 as functions of depth. We divide the viscous modes into two groups. For both earth models, the first group (modes M0 and L0) is associated with the boundary between the lithosphere and the mantle ($z = 110$ km). The second group (modes MC, LC, $L1_1$ and $L1_2$) appears only for earth model VC and is associated with the boundaries at the top ($z = 35$ km) and base ($z = 45$ km) of the lower crust.

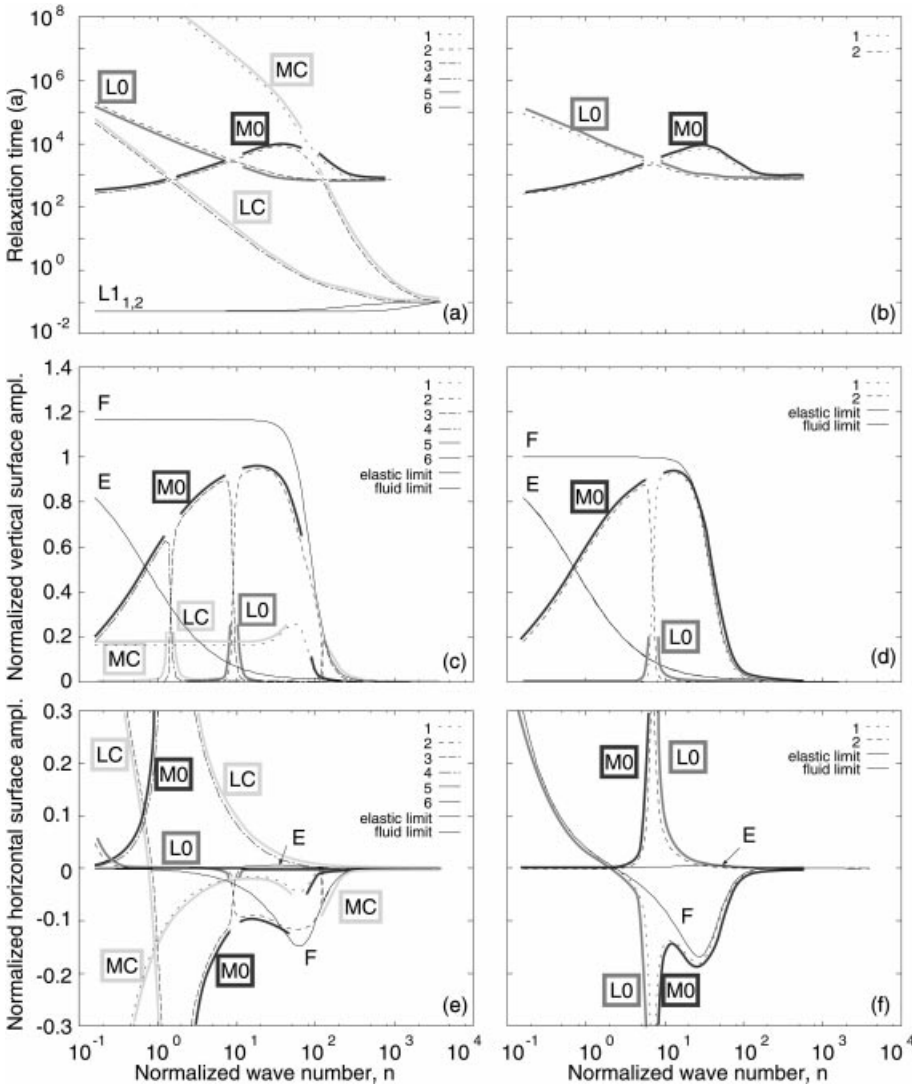

Figure 1. (a), (b) Relaxation times, (c), (d) normalized vertical surface amplitudes and (e), (f) normalized horizontal surface amplitudes as functions of normalized wavenumber. The calculations apply to earth model VC (left) and earth model EC (right). The surface amplitudes are normalized according to eqs (2) and (3) and the wavenumber according to $n := ka$, where a is the earth's radius. The symbols M0, MC, L0, LC and $L1_{1,2}$ denote the viscous modes; the symbols E and F denote the elastic and fluid amplitudes, respectively.

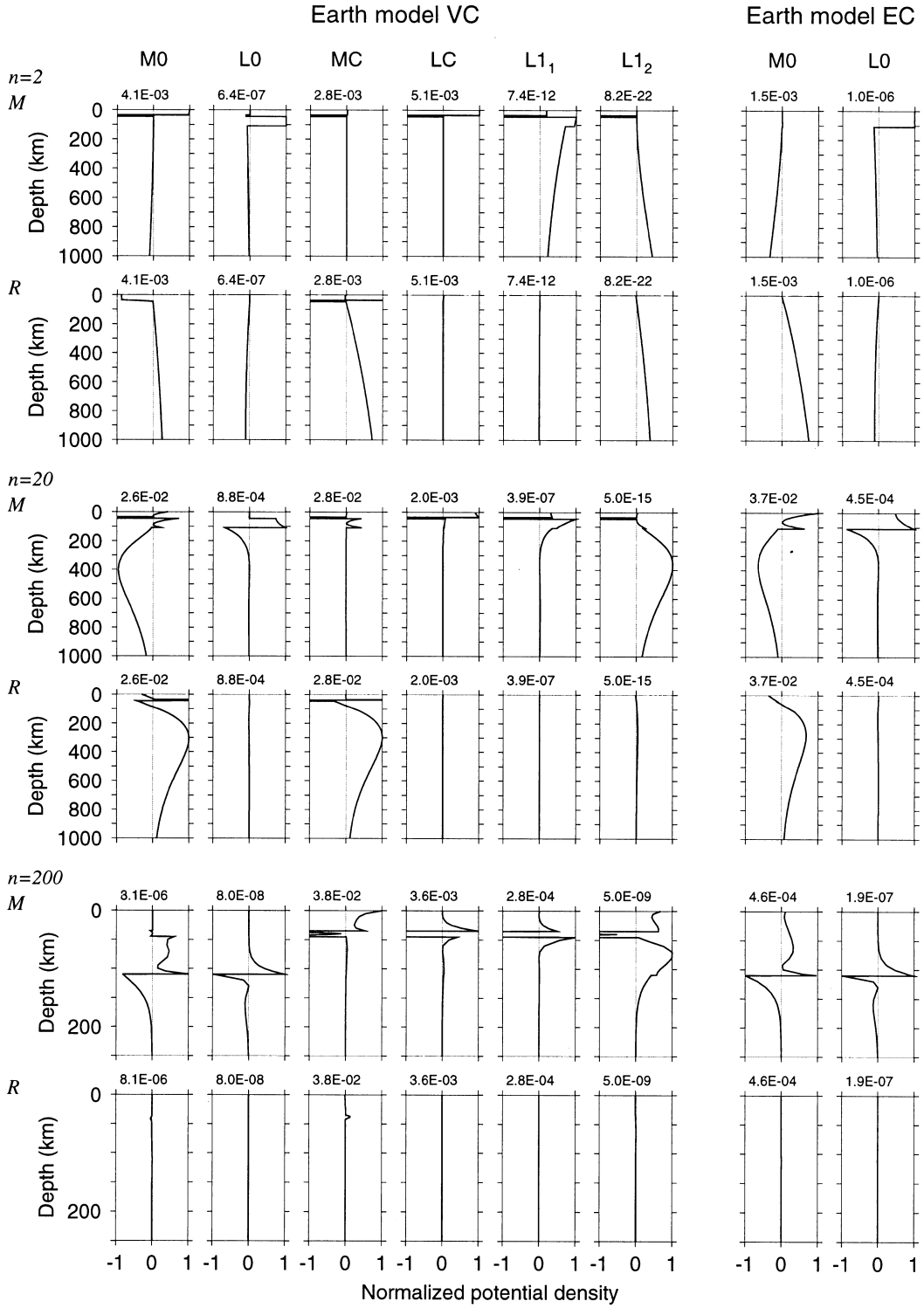

Figure 2. Shear- and gravitational-potential densities, M and R, of the viscous modes M0, L0, MC, LC, $L1_1$ and $L1_2$ for earth model VC (left) and earth model EC (right) and for the normalized wavenumbers 2, 20 and 200 as a function of depth. The potential densities are normalized with respect to the absolute maximum outside the ductile crustal layer, whose value is given at the top of each graph.

Starting with the first group, mode M0 is found to be confined mainly to the upper mantle, where, for $n=2$, 20, $M(z)$ and $R(z)$ have similar magnitudes but opposite signs. This classifies M0 as a buoyancy mode (e.g. Wu & Peltier 1982; Wolf 1985). For mode L0, $M(z)$ has smaller magnitude in the mantle than in the lithosphere and is strongly focused on the boundary between the lithosphere and the mantle. In contrast to this is the behaviour of $R(z)$, which is generally small in magnitude. This indicates that mode L0 is hardly affected by buoyancy and is therefore a viscoelastic mode. For $n=200$, $R(z)$ is almost zero for modes M0 and L0, and $M(z)$ is focused on the boundary between the lithosphere and the mantle. This suggests that

mode M0 no longer be classified as a buoyancy mode. It is interesting to note at this point that, if $R(z)$ vanishes identically for a particular viscous mode, the contributions of $M(z)$ must cancel each other for this mode according to eqs (A2), (A6) and (A7).

In the second group of modes, $M(z)$ for mode MC is confined mainly to the lower crust, whereas $R(z)$ for this mode has similar magnitude in the mantle as for mode M0. This classifies mode MC as an additional buoyancy mode. The behaviour of $M(z)$ for mode LC is comparable to that for mode L0, but $M(z)$ is now confined to the upper crust. With $R(z)$ nearly vanishing for all wavenumbers, this classifies mode LC as a further viscoelastic mode. The potential densities for modes $L1_1$ and $L1_2$ may not be confined to the lower crust, and for $n=2$, $L1_2$ shows the characterstics of a buoyancy mode. However, the magnitudes of the potential densities are usually much smaller than those for the other modes. Only for $n=200$ does the magnitude of $M(z)$ for mode $L1_1$ become more significant, and the depth dependence is similar to that for mode LC.

When studying the relaxation-time spectra (Figs 1a and b), we identify the modes M0 and L0 of the first group for both earth models. More interesting is the second group, in particular mode MC, for which the relaxation times for low wavenumbers are extremely long despite its association with the lower crust, whose Maxwell time, η_{LC}/μ_{LC}, is < 1 yr (Fig. 1a). The relaxation times of the pair of modes $L1_1$ and $L1_2$ appearing for earth model VC are close to the Maxwell time of the lower crust.

The significance of mode MC for glacial–isostatic adjustment processes can be understood from a discussion of the amplitude spectra for vertical displacement (Figs 1c and d). Particularly instructive is the consideration of the fluid amplitude for low wavenumbers. For earth model EC, it is simply the sum of the elastic amplitude and the viscous amplitude associated with the buoyancy mode M0 supported by the upper mantle with density ρ_{UM}. Quite different is earth model VC, for which the fluid amplitude for low wavenumbers is also controlled by the buoyancy mode MC. This mode is supported by the lower crust with the smaller density ρ_{LC}, resulting in an amplification of the fluid amplitude by a factor ρ_{UM}/ρ_{LC}. The long relaxation times of mode MC for small wavenumbers are related to the small relative thickness of the lower crust at these wavenumbers, which limits the lateral displacement rates for the material inside the ductile 'channel' (e.g. Kruse *et al.* 1991). In view of the shallow depth of the lower crust, mode MC is even more strongly excited at high wavenumbers of $n \sim 100$, where, however, the fluid amplitude is reduced due to the flexural rigidity of the elastic upper crust.

The main feature in the amplitude spectra for horizontal displacement (Figs 1e and f) is the appearance of peaks in the viscous amplitudes at wavenumbers for which an interchange of two modes takes place (Wolf *et al.* 1997). However, the contributions of the individual peaks largely cancel each other in view of the similar relaxation times of the modes near these wavenumbers. For both earth models, the elastic amplitudes are almost negligible. The behaviour of the viscous amplitudes for $n \to 0$ represents a simple pole, which is suppressed by the double root of the Hankel kernel $J_1(kr)k$ for $k = n/a \to 0$ when transformed back into the spatial domain.

Further insight into the significance of the viscoelastic lower crust and the implication of modes M0 and MC can be gained by studying the time dependence of the vertical displacement for a Heaviside loading event. This is shown in Fig. 3 for earth models VC and EC at the surface ($z=0$) and at the top of the mantle lithosphere ($z=45$ km).

For both earth models and for $n=2$ and $n=20$, the vertical surface displacement is initially controlled by mode M0. However, for earth model VC, the long relaxation times associated with mode MC result in an additional adjustment, with the vertical surface displacement increasing from a value of 1 to the value ρ_{UM}/ρ_{LC} between 10^6 and 10^8 yr after the onset of the loading. For both earth models and for $n=2$ and $n=20$, the mantle lithosphere initially follows the surface displacement, but for earth model VC, mode MC again becomes important after $\sim 10^6$ yr. In contrast to the surface, the amplitudes of modes M0 and MC are now of opposite sign, such that the top of the mantle lithosphere returns to its initial position in the fluid limit. This is a consequence of the rebound of the mantle lithosphere and the upper mantle. For $n=200$, the relaxation times of modes M0 and MC in earth model VC are very similar. However, as a consequence of the flexural rigidity of the elastic upper crust in earth model VC, the normalized vertical surface displacement reaches only a value of ~ 0.05 in the fluid limit, whereas, due to the decoupling of the upper crust from the mantle lithosphere, the vertical displacement at the top of the mantle lithosphere still vanishes in this limit. In contrast to this is the behaviour of earth model EC for $n=200$. Now, the mantle lithosphere is coupled to the upper crust and, therefore, follows the surface. In view of the larger flexural rigidity of the purely elastic lithosphere, the displacements are, however, further reduced and the normalized vertical surface displacement only reaches a value of ~ 0.01.

4 COMPUTATIONAL RESULTS: SPATIAL DOMAIN

We now compare the responses of earth models VC and EC in the spatial domain. As an example, we consider the Pleistocene Fennoscandian glaciations, which are simulated using an axisymmetric load model. In particular, we assume a sequence of 10 glaciations, where each has a duration of 100 kyr with a linear increase in load volume lasting 90 kyr and a linear decrease lasting 10 kyr. The load cross-section is taken as parabolic and the axial load thickness for the glacial maxima, h_L, is assumed to be 2200 m, corresponding to an axial load pressure of ~ 20 MPa. Except for the last glaciation, the load radius, r_L, is kept fixed at 1000 km. During the last deglaciation, the load volume is reduced in five steps, where the radius and thickness are varied such that $h_L^2/r_L = \text{constant}$ applies (Fig. 4). The present time (PT) is assumed to correspond to $t=0$, the end of deglaciation (EOD) is taken at $t=-8$ kyr and the last glacial maximum (LGM) at $t=-18$ kyr.

We begin by studying the consequences of a viscoelastic lower crust for the change of deformation. Considering the rate of vertical displacement at the PT first, we notice that its value is only slightly affected by the presence of the viscoelastic lower crust (Fig. 5a). This is because the contribution of a mode to the rate of change is inversely proportional to the relaxation time of the mode and is thus much smaller for mode MC than for mode M0 at the dominant wavenumbers around $n=20$ in the load spectrum near the LGM. The rather large difference between the horizontal displacement rates at the PT for

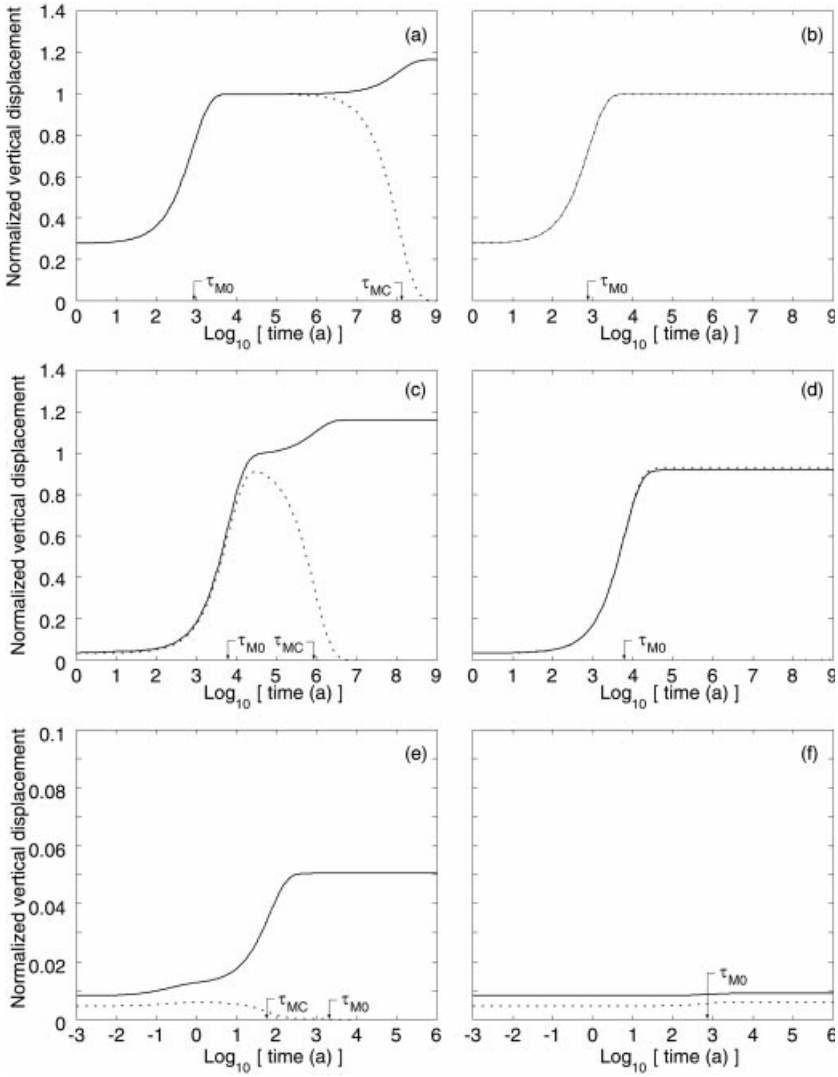

Figure 3. Normalized vertical displacement as a function of time after emplacement of a Heaviside load for the normalized wave numbers (a), (b) 2, (c), (d) 20 and (e), (f) 200 at the surface (solid) and the base of the crust (dashed). The calculations apply to earth model VC (left) and earth model EC (right). The symbols τ_{M0} and τ_{MC} denote the relaxation times of modes M0 and MC.

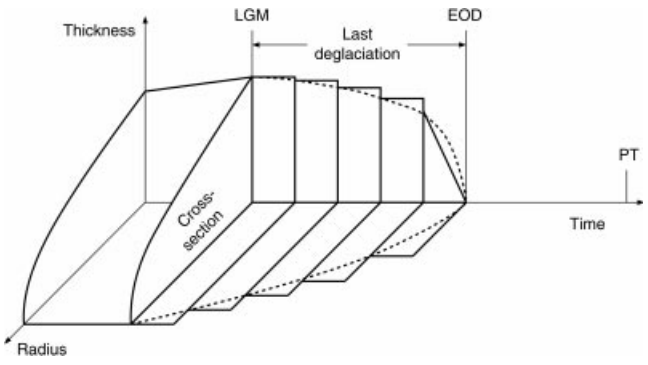

Figure 4. Decrease of load thickness and load radius according to h_L^2/r_L = constant for a linear reduction of load volume during the last deglaciation (dashed) and discretization of load thickness and load radius used (solid). The abbreviations LGM, EOD and PT denote last glacial maximum, end of deglaciation and present time, respectively.

earth models VC and EC (Fig. 5b) is related to the more complicated spectra of the horizontal amplitudes (Figs 1e and f). Unfortunately, the usefulness of this quantity for inferring a ductile layer is restricted by its similarly strong sensitivity to lateral heterogeneities (Gasperini *et al.* 1990).

Next, we consider the gravity signatures associated with the deformation at the PT. For the free-air gravity anomaly (referred to a fixed *spatial point*, Fig. 6a), we find that the presence of a viscoelastic lower crust in earth model VC causes a smaller effect than expected from the enhanced vertical surface displacement after 10 glaciations (Fig. 3). This is because, for earth model VC, the cumulative forcing of the 10 glaciations simultaneously produces a reduced vertical displacement of the denser mantle lithosphere (Fig. 3), which partially compensates for the additional surface contribution. The relaxation of the additional vertical displacement in earth model VC after the LGM proceeds on the long timescale of mode MC and is, therefore, very small at the PT. In consequence

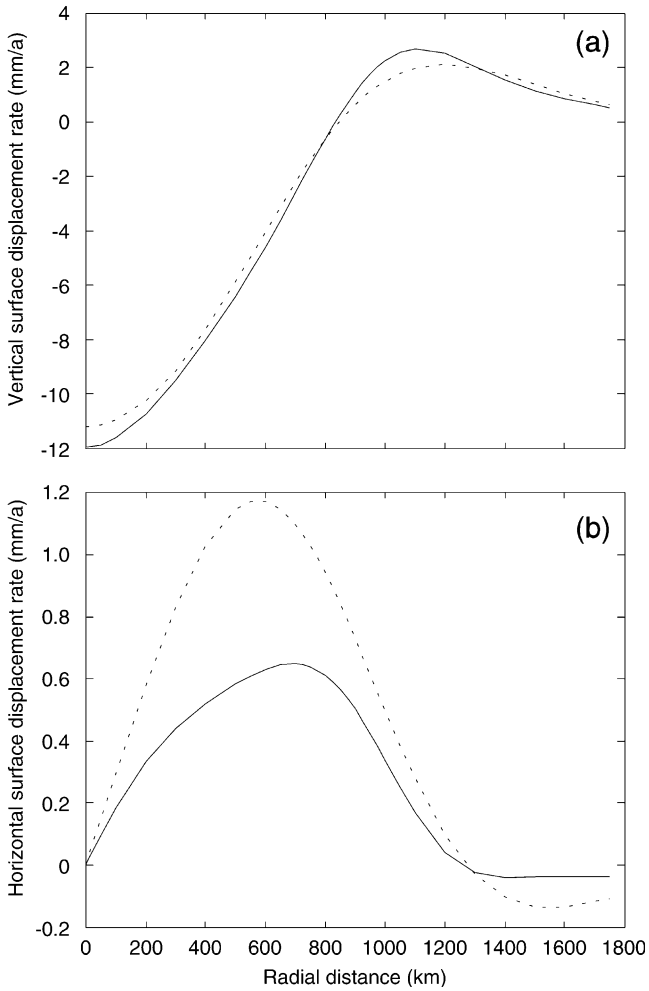

Figure 5. (a) (Downward) vertical surface displacement rate and (b) (outward) horizontal surface displacement rate at the PT as functions of radial distance with respect to the load axis. The calculations apply to earth model VC (solid), earth model EC (dashed) and an axisymmetric load model simulating 10 Fennoscandian glaciations (see the text).

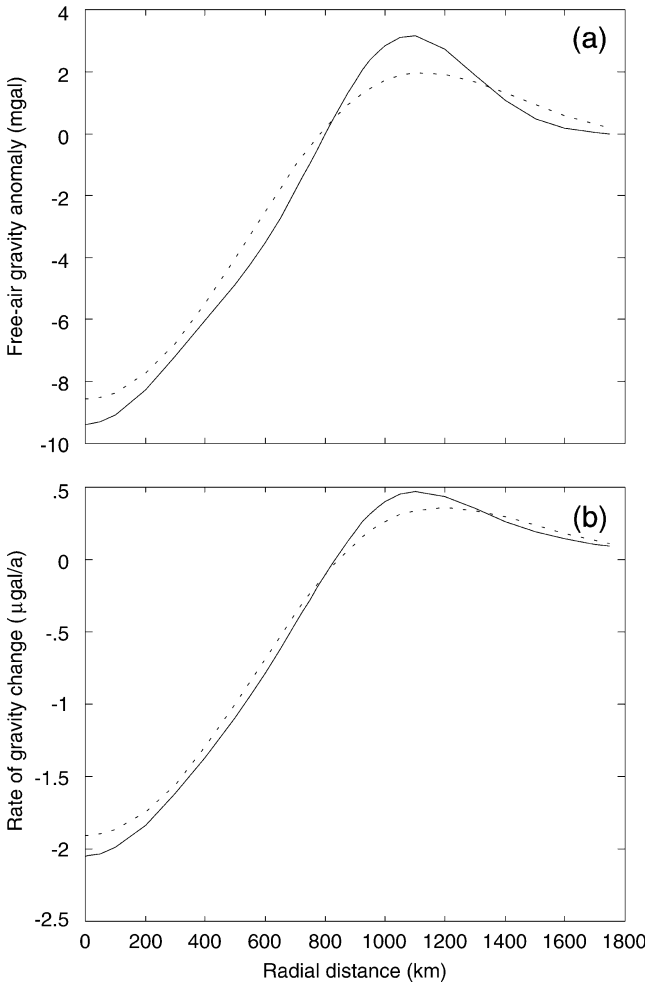

Figure 6. (a) Free-air gravity anomaly and (b) rate of gravity change at the PT as functions of radial distance from the load axis. The calculations apply to earth model VC (solid), earth model EC (dashed) and an axisymmetric load model simulating 10 Fennoscandian glaciations (see the text).

of this, the rate of gravity change (referred to a fixed *material point*) is only slightly affected by mode MC (Fig. 6b) and the difference between earth models EC and VC is similar to that found for the vertical displacement rate (Fig. 5a).

A further observable associated with the deformation is the stress. A convenient measure of its deviation from the hydrostatic stress belonging to the unperturbed initial state is the maximum shear stress defined by $t_{SS} := (t_{max} - t_{min})/2$, where t_{max} and t_{min} are the maximum and minimum principal stresses, respectively. At the LGM, the partition into two distinct elastic layers in earth model VC is clearly reflected by t_{SS} (Fig. 7a). In the upper crust, the stress field is typical of a flexed elastic layer superimposed on a fluid substratum (e.g. Klemann & Wolf 1998). The distribution is thus nearly symmetric with respect to the median plane of the upper crust, with pairs of maxima located near the load margin. In the mantle lithosphere, the symmetry is similar but the maxima are smaller. The intervening lower crust is characterized by a hydrostatic stress field. We note that such a decoupling of the elastic layers was not found by Wu (1997). The reason for this difference in behaviour is that he used a viscosity of 10^{22} Pa s for the ductile layer, which is higher than the viscosity of 10^{21} Pa s in the mantle. The distribution of t_{SS} in the purely elastic lithosphere of earth model EC at the LGM shows the pattern expected for a flexed elastic layer superimposed on a fluid substratum (Fig. 7b). At the EOD, the symmetries are largely destroyed for both earth models, but the decoupling of the two elastic layers by the lower crust in earth model VC is preserved (Figs 7c and d). At the PT, the maxima of t_{SS} have decreased to values of 2–3 MPa. Near the surface, the stress distributions are similar for both earth models. However, in view of the long relaxation time of mode MC, larger stress values are reached near the top and base of the mantle lithosphere in earth model VC (Figs 7e and f).

Of interest are the implications of the stress field for seismicity. This can be quantified in terms of the incremental fault stability margin (FSM), which is a measure of the load-induced increase in the difference between the failure stress according to Coulomb's law and the maximum shear stress (Johnston 1989). Thus, positive values of the incremental FSM indicate increasing stability and negative values decreasing stability. The important features of the evolution of the

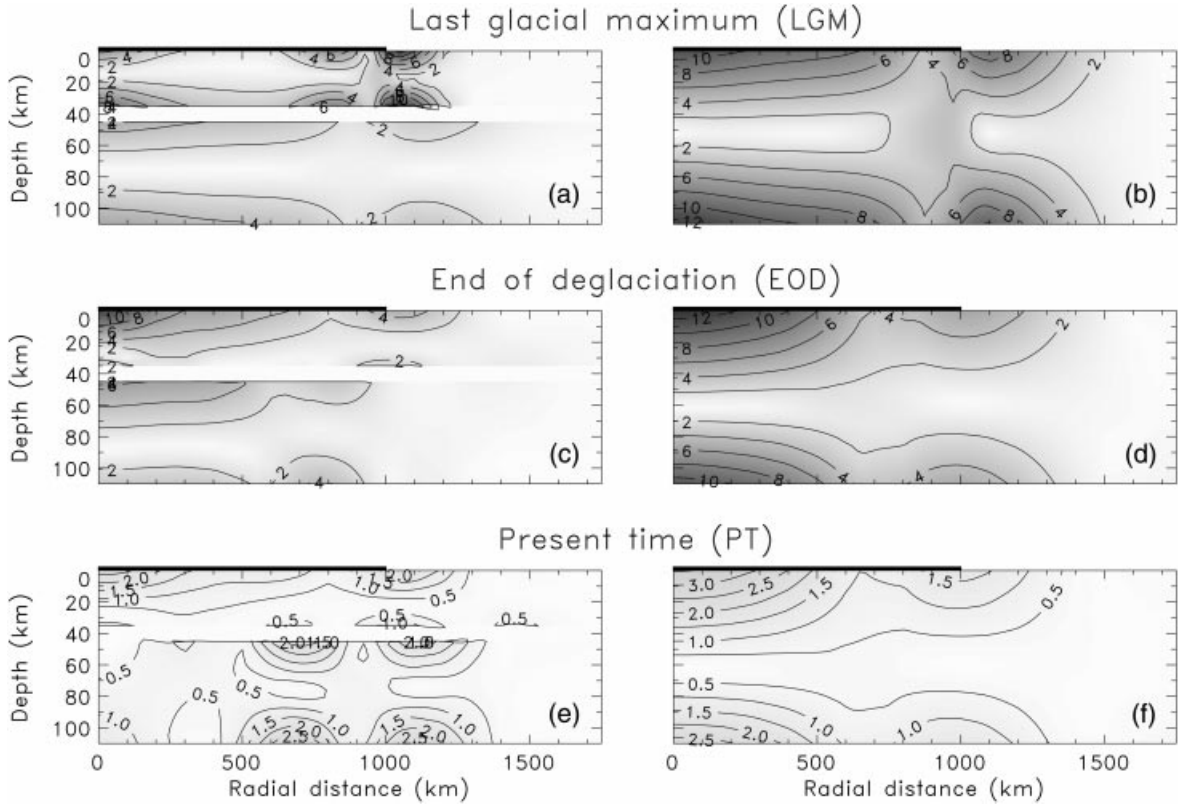

Figure 7. Maximum shear stress in units of MPa as a function of radial distance and depth for the epochs considered. The calculations apply to earth model VC (left), earth model EC (right) and an axisymmetric load model simulating 10 Fennoscandian glaciations (see the text). The black bars indicate the extension of the load at the LGM.

incremental FSM near the surface are (1) stabilization during loading (Johnston 1987) and (2) destabilization after load removal, even for locations that are initially stable (Wu & Hasegawa 1996a,b; Johnston *et al.* 1998). For the load model used in the present study, the destabilization takes place for earth model VC ~1 kyr later than for earth model EC (Figs 8a and b). Also of interest are the *load-induced* stress regimes (Figs 8c and d). Since the *total* stress field in Fennoscandia is dominated by compressive *tectonic* stress oriented NW–SE (e.g. Grünthal & Stromeyer 1992), the thrust regimes indicated below the load at the PT enhance the tendency towards thrust faulting. In contrast to this are the strike-slip and extension regimes indicated near the load margin, which are at variance with the compressive tectonic stress regime and, therefore, not expected to support strike-slip and normal faulting, respectively, in its presence.

This is confirmed by Figs 9 and 10, which show the effects caused by a *linear superposition* of the load-induced stress field and a homogeneous tectonic stress field with values of ~50 and ~45 MPa for the maximum and minimum horizontal principal compressive stresses, p_{Hmin} and p_{Hmax}, respectively. To show the extreme effects, the evolution of the incremental FSM and of the stress regimes is plotted for a profile oriented NW–SE, that is, collinear to p_{Hmax} (Fig. 9), and for a profile oriented NE–SW, that is, perpendicular to p_{Hmax} (Fig. 10). For both orientations, the extension and strike-slip regimes associated with the load-induced stresses near the load margin (Figs 8c and d) are now characterized by stability. Thus, only the thrust regime below the load after the EOD is retained. The interval of instability continues until the PT around the load axis but ends slightly earlier than without tectonic stress near the load margin. A comparison of Figs 9 and 10 shows that the differences arising from the orientation of the profile relative to the tectonic stress are small.

Comparing the behaviour of the two earth models in Figs 9 and 10, we find results similar to those found by Wu (1997). Thus, for earth model VC, the space–time region of negative incremental FSM is larger and, near the load margin, the interval of negative incremental FSM is longer than for model EC (Figs 9c and d and 10c and d). On the other hand, the magnitudes of the incremental FSM are smaller for earth model VC than for earth model EC as a result of the faster stress relaxation near the surface for earth model VC (Figs 9a and b and 10a and b).

5 CONCLUDING REMARKS

The main results of the present study are as follows.

(1) A comparison of the relaxation-time and amplitude spectra of the layered Maxwell viscoelastic earth models VC and EC shows that a viscoelastic lower crust simulating a ductile crustal layer supports a slowly decaying mode MC, which is capable of markedly modifying the deformation associated with the conventional mode M0 present in both earth models.

(2) For a simple model of the sequence of glaciations in Fennoscandia during the Pleistocene, the results in the space–time domain for measures of the *absolute* deformation such as the free-air gravity anomaly and the stress field are expected to

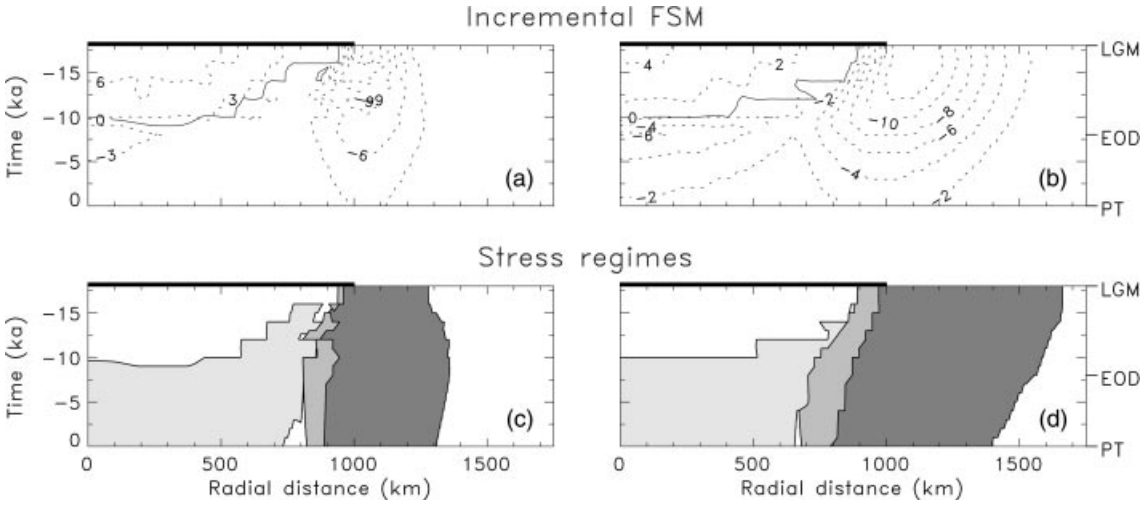

Figure 8. (a), (b) Incremental FSM and (c), (d) stress regimes at the surface as functions of radial distance and time with respect to the PT for a hydrostatic initial stress. The calculations apply to earth model VC (left), earth model EC (right) and an axisymmetric load model simulating 10 Fennoscandian glaciations (see the text). The black bars indicate the extension of the load at the LGM. The numbers on the contours give the incremental FSM in units of MPa. Light grey shades indicate thrust regimes, medium grey shades strike-slip regimes, dark grey shades extensional regimes and white shades space–time regions of positive incremental FSM.

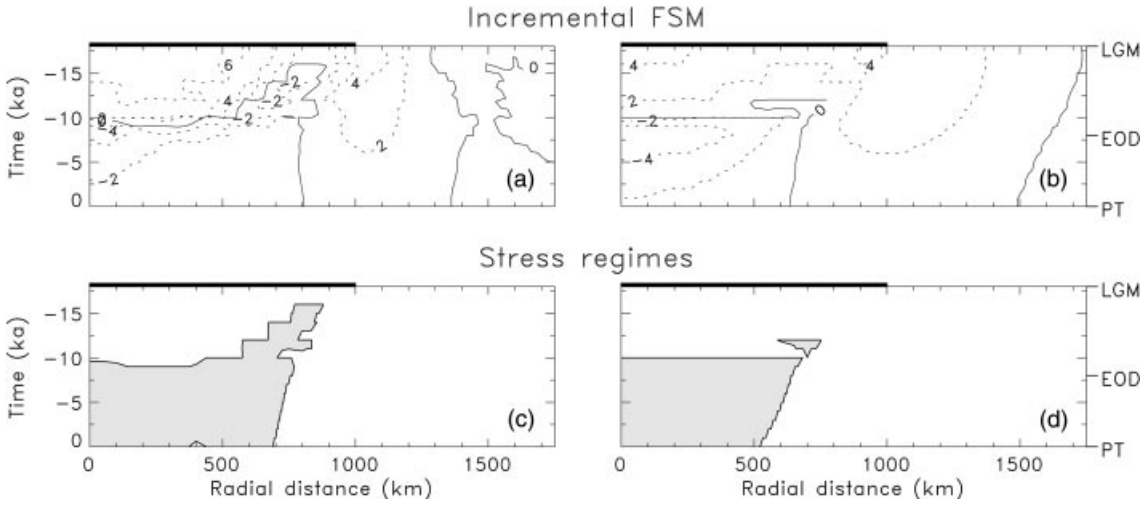

Figure 9. As for Fig. 8 but including a superimposed homogeneous tectonic stress with maximum and minimum horizontal compressive stresses of $p_{\mathrm{Hmax}} = 50$ MPa and $p_{\mathrm{Hmin}} = 45$ MPa and a profile oriented collinear to p_{Hmax}.

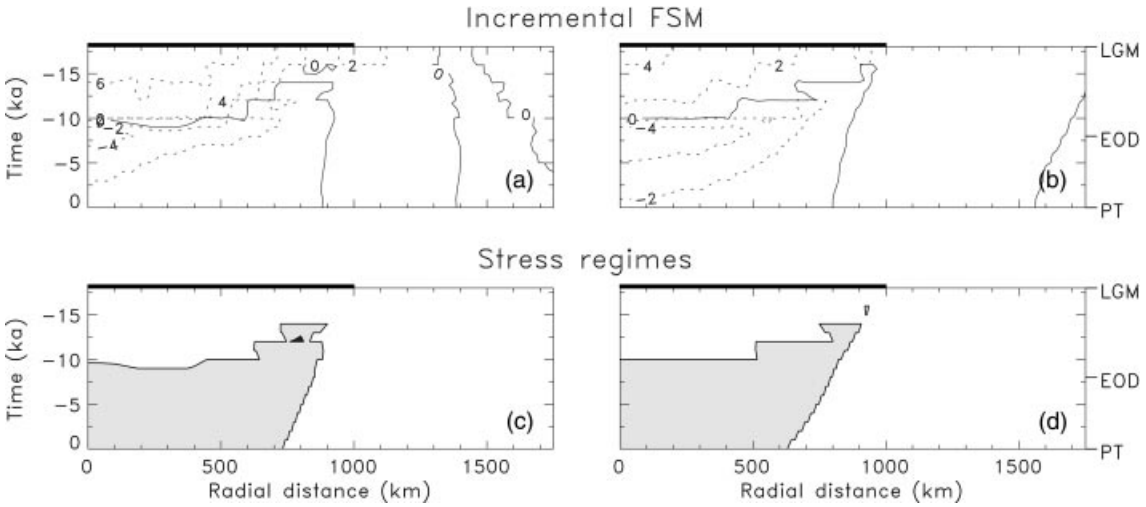

Figure 10. As for Fig. 8 but including a superimposed homogeneous tectonic stress with maximum and minimum horizontal compressive stresses of $p_{\mathrm{Hmax}} = 50$ MPa and $p_{\mathrm{Hmin}} = 45$ MPa and a profile oriented perpendicular to p_{Hmax}.

reflect the presence of a ductile crustal layer. This is confirmed for the stress field. For the free-air gravity anomaly, the contributions resulting from the vertical displacements at the surface and at the top of the mantle lithosphere partially cancel each other and therefore mask the differences in deformational behaviour between the two earth models.

(3) In contrast to this are measures of the *relative* deformation such as the rates of vertical displacement and gravity change. In good approximation, they are inversely proportional to the relaxation times of the more quickly decaying mode M0 and thus less affected by a ductile crustal layer.

(4) Taken together, the results suggest that, provided a ductile crustal layer exists, its presence should be accounted for in interpretations of the glacial–isostatic adjustment.

ACKNOWLEDGMENTS

We would like to thank Jeroen Tromp and Jerry Mitrovica for making available to us two manuscripts before publication and Jerry Mitrovica and Patrick Wu for constructive comments. The research of VK was supported by a graduate scholarship of the German Research Foundation (DFG).

REFERENCES

Arvidsson, R., 1996. Fennoscandian earthquakes: whole crustal rupturing related to postglacial rebound, *Science,* **274,** 744–746.

Backus, G.E. & Gilbert, J.F., 1967. Numerical applications of a formalism for geophysical inverse problems, *Geophys. J. R. astr. Soc.,* **13,** 247–276.

Breuer, D. & Wolf, D., 1995. Deglacial land emergence and lateral upper-mantle heterogeneity in the Svalbard Archipelago—I. First results for simple load models, *Geophys. J. Int.,* **121,** 775–788.

Chen, W.-P. & Molnar, P., 1983. Focal depths of intracontinental and intraplate earthquakes and their implications for the thermal and mechanical properties of the lithosphere, *J. geophys. Res.,* **88,** 4183–4214.

De Rito, R.F., Cozzarelli, F.A. & Hodge, D.S., 1986. A forward approach to the problem of nonlinear viscoelasticity and the thickness of the mechanical lithosphere, *J. geophys. Res.,* **91,** 8295–8313.

Gasperini, P., Yuen, D.A. & Sabadini, R., 1990. Effect of lateral viscosity variations on postglacial rebound: implications for recent sea-level trends, *Geophys. Res. Lett.,* **17,** 5–8.

Grünthal, G. & Stromeyer, D., 1992. The recent crustal stress field in Central Europe: trajectories and finite element modeling, *J. geophys. Res.,* **97,** 11 805–11 820.

Johnston, A.C., 1987. Suppression of earthquakes by large continental ice sheets, *Nature,* **330,** 467–469.

Johnston, A.C., 1989. The effect of large ice sheets on earthquake genesis, in *Earthquakes at North-Atlantic Passive Margins: Neotectonics and Postglacial Rebound,* pp. 581–599, eds Gregersen, S. & Basham, P.W., Kluwer Academic, Dordrecht.

Johnston, P., Wu, P. & Lambeck, K., 1998. Dependence of horizontal stress magnitude on load dimension in glacial rebound models, *Geophys. J. Int.,* **132,** 41–60.

Kaufman, P.S. & Royden, L.H., 1994. Lower crustal flow in an extensional setting: constraints from the Halloran Hill region, eastern Mojave Desert, California, *J. geophys. Res.,* **99,** 15 723–15 739.

Klein, A., Jacoby, W. & Smilde, P., 1997. Mining-induced crustal deformation in Northwest Germany: modelling the rheological structure of the lithosphere, *Earth planet. Sci. Lett.,* **147,** 107–123.

Klemann, V. & Wolf, D., 1998. Modelling of stresses in the Fennoscandian lithosphere induced by Pleistocene glaciations, *Tectonophysics,* **294,** 291–303.

Kohlstedt, D.L., Evans, B. & Mackwell, S.J., 1995. Strength of the lithosphere: constraints imposed by laboratory experiments, *J. geophys. Res.,* **100,** 17 587–17 602.

Kruse, S., McNutt, M., Phipps-Morgan, J., Royden, L. & Wernicke, B., 1991. Lithospheric extension near Lake Mead, Nevada: a model for ductile flow in the lower crust, *J. geophys. Res.,* **96,** 4435–4456.

Lobkovsky, L.L. & Kerchman, V.I., 1991. A two-level concept of plate tectonics: application to geodynamics, *Tectonophysics,* **199,** 343–374.

Meissner, R. & Strehlau, J., 1982. Limits of stresses in continental crusts and their relation to the depth–frequency distribution of shallow earthquakes, *Tectonics,* **1,** 73–89.

Meissner, R. & Wever, T., 1986. Nature and development of crust according to deep reflection data from the German Variscides, in *Reflection Seismology: A Global Perspective, Geodynamics Series,* Vol. 13, pp. 31–42, eds Barazangi, M. & Brown, L., AGU, Washington.

Peltier, W.R., 1976. Glacial–isostatic adjustment—II. The inverse problem, *Geophys. J. R. astr. Soc.,* **46,** 669–705.

Ranalli, G. & Murphy, D.C., 1987. Rheological stratification of the lithosphere, *Tectonophysics,* **132,** 281–295.

Rydelek, P.A. & Pollitz, F.F., 1994. Fossil strain from the 1811–1812 New Madrid earthquakes, *Geophys. Res. Lett.,* **21,** 2303–2306.

Rydelek, P.A. & Sacks, I.S., 1990. Asthenospheric viscosity and stress diffusion: a mechanism to explain correlated earthquakes and surface deformations in NE Japan, *Geophys. J. Int.,* **100,** 39–58.

Slunga, R.S., 1989. Focal mechanisms and crustal stresses in the Baltic Shield, in *Earthquakes at North-Atlantic Passive Margins: Neotectonics and Postglacial Rebound,* pp. 261–276, eds Gregersen, S. & Basham, P.W., Kluwer Academic, Dordrecht.

Tromp, J. & Mitrovica, J.X., 1999a. Surface loading of a viscoelastic Earth—I. General theory, *Geophys. J. Int.,* **137,** 847–855.

Tromp, J. & Mitrovica, J.X., 1999b. Surface loading of a viscoelastic Earth—II. Spherical models, *Geophys. J. Int.,* **137,** 856–872.

Vetter, U.R. & Meissner, R.O., 1979. Rheological properties of the lithosphere and applications to passive continental margins, *Tectonophysics,* **59,** 367–380.

Weertman, J., 1978. Creep laws for the mantle of the Earth, *Phil. Trans. R. Soc. Lond.,* A, **288,** 9–26.

Wolf, D., 1985. The normal modes of a layered, incompressible Maxwell half-space, *J. Geophys.,* **57,** 106–117.

Wolf, D., 1991. Boussinesq's problem of viscoelasticity, *Terra Nova,* **3,** 401–407.

Wolf, D., Barthelmes, F. & Sigmundsson, F., 1997. Predictions of deformation and gravity change caused by recent melting of the Vatnajökull ice cap, Iceland, in *Gravity, Geoid and Marine Geodesy,* pp. 311–319, eds Segawa, J., Fujimoto, H. & Okubo, S., Springer-Verlag, Berlin.

Woodhouse, J.H., 1976. On Rayleigh's principle, *Geophys. J. R. astr. Soc.,* **46,** 11–22.

Wu, P., 1997. Effects of viscosity structure on fault potential and stress orientations in eastern Canada, *Geophys. J. Int.,* **130,** 365–382.

Wu, P. & Hasegawa, H.S., 1996a. Induced stresses and fault potential in eastern Canada due to a disc load: a preliminary analysis, *Geophys. J. Int.,* **125,** 415–430.

Wu, P. & Hasegawa, H.S., 1996b. Induced stresses and fault potential in eastern Canada due to a realistic load: a preliminary analysis, *Geophys. J. Int.,* **127,** 215–229.

Wu, P. & Peltier, W.R., 1982. Viscous gravitational relaxation, *Geophys. J. R. astr. Soc.,* **70,** 435–485.

APPENDIX A: CALCULATION OF THE POTENTIAL DENSITIES

Following Tromp & Mitrovica (1999a), we define a variational equation, $J[\boldsymbol{u}] := (\mathbf{L}\boldsymbol{u}, \boldsymbol{u})/2$, by the inner product $(\boldsymbol{u}, \boldsymbol{v}) := \int_V \boldsymbol{u} \cdot \boldsymbol{v}^* \, d^3X$, where $\boldsymbol{u}, \boldsymbol{v} \in \mathrm{C}^2(V)$, which is the space of twice

continuously differentiable functions on the volume V. The symbol L is the Hermitian differential operator of a homogeneous differential equation, $\mathbf{L}\boldsymbol{u}=\mathbf{0}$, $\boldsymbol{u}$ is an eigenfunction of it and the asterisk denotes the conjugate complex. If L$\boldsymbol{u}$ is the momentum equation, this form of J leads to the (physical) *Lagrangian* in terms of the energy densities (e.g. Backus & Gilbert 1967; Woodhouse 1976).

In our problem, the linear differential operator, L, is defined by the Laplace-transformed momentum and constitutive equations for a homogeneous, incompressible Maxwell viscoelastic fluid. Indicating Laplace transformation by a tilde and using tensor notation, it takes the form (e.g. Wolf 1985, 1991)

$$[\mathbf{L}\tilde{\boldsymbol{u}}]_i := -\tilde{p}_{,j}\,\delta_{ij}+\tilde{\mu}\,\tilde{u}_{i,jj}+\tilde{\mu}\,\tilde{u}_{j,ji}+\rho\,g\,\delta_{j3}\,\tilde{u}_{j,i}=0\,. \tag{A1}$$

Under homogeneous boundary conditions, the operator L is self-adjoint and the displacement, $\tilde{u}_i$, is an eigenfunction (e.g. Tromp & Mitrovica 1999a). The first three terms of the sum in eq. (A1) represent the viscoelastic force with $\tilde{p}$ the material incremental pressure, δ_{ij} the Kronecker symbol and $\tilde{\mu}:=\tilde{m}_2\sigma$ the product of the shear-relaxation function, $\tilde{m}_2$, and an eigenvalue, σ. The last term of the sum represents the buoyancy force with ρ the density and g the gravity.

Evaluating the variational equation, $J[\tilde{\boldsymbol{u}}]$, under consideration of eq. (A1), we may separate contributions involving $\tilde{\mu}$ and ρ, respectively, by defining the shear potential, $\mathscr{E}_\mu$, and the gravitational potential, $\mathscr{E}_\rho$, where

$$\mathscr{E}_\mu+\mathscr{E}_\rho=0 \tag{A2}$$

applies to each eigenfunction $\tilde{u}_i$ (Tromp & Mitrovica 1999a). The shear and gravitational potentials take the forms

$$\mathscr{E}_\mu=\int_V \tilde{\mu}\,\tilde{\epsilon}_{ij}\,\tilde{\epsilon}_{ij}\,d^3X\,, \tag{A3}$$

$$\mathscr{E}_\rho=-\frac{1}{2}\int_V \rho\,g\,\delta_{j3}\,\tilde{u}_{j,i}\,\tilde{u}_i\,d^3X\,, \tag{A4}$$

where $\tilde{\epsilon}_{ij}:=(\tilde{u}_{j,i}+\tilde{u}_{i,j})/2$ is the strain and the asterisk has been dropped because all quantities are real. Note that the integrand in eq. (A3) formally agrees with the shear energy density for the elastic case (Woodhouse 1976).

In the following, the potentials are calculated in cylindrical coordinates (r, φ, z) for the mth viscous amplitude in terms of the displacement components U_m^{V} and W_m^{V}. Assuming axisymmetric perturbations, we have

$$\tilde{\boldsymbol{u}}_m := U_m^{\mathrm{V}}\mathrm{J}_1(kr)\,\boldsymbol{e}_r+W_m^{\mathrm{V}}\mathrm{J}_0(kr)\,\boldsymbol{e}_z\,, \tag{A5}$$

where $\mathrm{J}_n(kr)$ is the Bessel function of the first kind and nth order and $\boldsymbol{e}_r$ and $\boldsymbol{e}_z$ are unit vectors in the positive r and z directions, respectively. Eq. (A5) represents the mth eigenfunction of eq. (A1) for a distinct wavenumber, k, in the spatial domain. The associated eigenvalue is $\sigma_m=-1/\tau_m$. The depth distributions of the potentials are given by (e.g. Peltier 1976; Tromp & Mitrovica 1999b)

$$\mathscr{E}_\mu=\int_0^\infty M(z)\,dz\,, \tag{A6}$$

$$\mathscr{E}_\rho=\int_0^\infty R(z)\,dz\,, \tag{A7}$$

where the potential densities, $M(z)$ and $R(z)$, are evaluated by inserting eq. (A5) into eqs (A3) and (A4) and integrating over the radial distance, r, and the azimuth, φ. Because the integral over r is not finite, the expressions are normalized with respect to $2\pi\int_0^\infty[\mathrm{J}_0(kr)]^2 r\,dr$. The equations for the potential densities of the mth eigenfunction for a distinct wavenumber then take the forms

$$M(z)=\tilde{\mu}\left\{2[kU_m^{\mathrm{V}}]^2+\frac{1}{2}\left[\frac{\partial}{\partial z}\,U_m^{\mathrm{V}}-kW_m^{\mathrm{V}}\right]^2\right\}, \tag{A8}$$

$$R(z)=\rho\{gkU_m^{\mathrm{V}}W_m^{\mathrm{V}}\}\,. \tag{A9}$$